Electron Transfer to Protonated β-Alanine N-Methylamide in the Gas Phase: An Experimental and Computational Study of Dissociation Energetics and Mechanisms

Chunxiang Yao, Erik A. Syrstad,† and František Tureček*

Department of Chemistry, Bagley Hall, Box 351700, University of Washington, Seattle, Washington 98195-1700

Received: January 20, 2007; In Final Form: March 13, 2007

Ammonium radicals derived from protonated β-alanine N-methyl amide (BANMA) were generated by femtosecond collisional electron transfer to gas-phase cations prepared by chemical ionization and electrospray. Regardless of the mode of precursor ion preparation, the radicals underwent complete dissociation on the time scale of 5.15 μs. Deuterium isotope labeling and product analysis pointed out several competitive and convergent dissociation pathways that were not completely resolved by experiment. Ab initio calculations, which were extrapolated up to the CCSD(T)/6-311++G(3df,2p) level of theory, provided the proton affinity and gas-phase basicity of BANMA as PA = 971 kJ mol^{-1} and GB = 932 kJ mol^{-1} to form the most stable ion structure **1c**$^+$ in which the protonated ammonium group was internally solvated by hydrogen bonding to the amide carbonyl. Ion **1c**$^+$ was calculated to have an adiabatic recombination energy of 3.33 eV to form ammonium radical **1c**•. The potential energy surface for competitive and consecutive isomerizations and dissociations of **1c**• was investigated at correlated levels of theory and used for Rice−Ramsperger−Kassel−Marcus (RRKM) calculations. RRKM unimolecular rate constants suggested that dissociations starting from the ground electronic state of radical **1c**• were dominated by loss of an ammonium hydrogen atom. In contrast, dissociations starting from the B excited state were predicted to proceed by reversible isomerization to an aminoketyl radical (**1f**•). The latter can in part dissociate by N−C_α bond cleavage leading to the loss of the amide methyl group. This indicates that apparently competitive dissociations observed for larger amide and peptide radicals, such as backbone cleavages and losses of side-chain groups, may originate from different electronic states and proceed on different potential energy surfaces.

Introduction

There has been much recent interest in exploring the dissociations of multiply protonated peptides and proteins following cation−electron and cation−anion recombinations in the gas phase. The recombination produces open-electron shell ions, called charge-reduced ions, that often undergo extensive dissociation by losses of small molecules and by side-chain and backbone cleavages. In addition to the analytical utility of these electron-capture (ECD)[1] and electron-transfer dissociations (ETD)[2] for peptide sequencing using mass spectrometry, they also raise interesting questions of reaction mechanisms,[3−5] energetics,[4−7] and dynamics.[8] One of the current ECD mechanisms for backbone cleavage in charge-reduced peptide ions presumes electron capture in the charge-carrying group followed by exothermic hydrogen transfer to a proximate amide group to form an aminoketyl radical intermediate.[3,4] These are known to be weakly bound[9] and dissociate by breaking the bond between the amide nitrogen atom and the adjacent α-carbon of the C-terminal residue (N−C_α bond cleavage),[7−10] as depicted in Scheme 1. The propensity for hydrogen transfer forming the labile aminoketyl intermediate has been studied by experiment and theory for hydrogen atom donors incorporating ammonium, guanidinium, and imidazolium groups (X in Scheme 1), which are relevant, respectively, to lysine,[4,7] arginine,[11] and histidine[12] amino acid residues in peptides and proteins. While the arginine[11] and histidine[12] residues were found to be inefficient hydrogen atom donors, previous calculations indicated that hydrogen atom transfer from the ammonium group in lysine and some other simple model compounds may be facile in that it was substantially exothermic and required only low activation energies.[4]

SCHEME 1

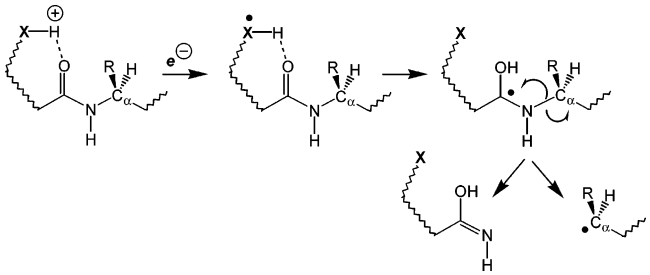

We now report a combined experimental and computational study of ETDs that uses β-alanine N-methyl amide (BANMA) as a model system. Protonated BANMA can be produced as a singly charged ammonium ion in the gas phase and is expected to have a well-defined structure including an intramolecular hydrogen bond to the amide carbonyl (Scheme 2). The gas-phase ion is neutralized by femtosecond nonresonant electron transfer from a suitable electron donor, and neutral products of dissociations ensuing from electron transfer are analyzed by mass spectrometry after nonselective collisional ionization to cations. This cation neutralization−cation reionization ($^+NR^+$) mass spectrometric method[13] provides practically complete

† Present address: Space Dynamics Laboratory, Utah State University, Logan, UT 84322.

10.1021/jp0705020 CCC: $37.00
Published on Web 04/25/2007

SCHEME 2

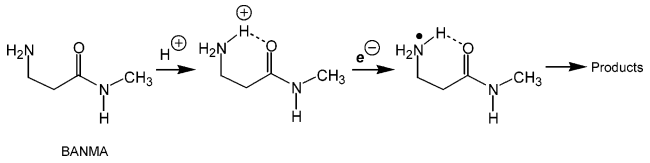

analysis of products of neutral dissociations and, when applied in combination with deuterium labeling, can be used to discuss the dissociation mechanisms. In addition, the small size of BANMA radicals (18 atoms) allows one to use high-level ab initio and density functional theory computations to obtain structures and energies for reactants, transition states, reaction intermediates, and products to elucidate the dissociation pathways in some detail.

It should be noted that whereas peptides and proteins are built up from α-amino acids that are linked to form $C-N_\alpha$ amide bonds, amides consisting of β-amino acids also appear in natural and synthetic peptides, proteins, and related compounds. For example, the base-catalyzed rearrangement of aspartic to isoaspartic residues in proteins results in the formation of β-amide bonds that are indicators of protein aging and degradation.[14] β-Peptoides are an example of biopolymers that incorporate β-alanine units to form a β-amide backbone.[15a] β-Alanine is a component of the skeletal muscle peptides anserine and carnosine[15b] and panthothenic acid,[15c] and β-alanine amide linkages also appear in various dendrimers, which show a strong binding ability for proton and protic solvents.[16]

Experimental Part

Materials and Methods. β-Alanine-N-methyl amide was prepared from β-alanine methyl ester hydrochloride according to the literature[17] as follows. NaOH (2.6 g, 65 mmol) was dissolved in 30 mL of methanol. The solution was cooled to 0 °C, and β-alanine methyl ester hydrochloride (98%, Sigma-Aldrich 3 g, 21.5 mmol) was added under stirring. The solution was then cooled to −20 °C in an ice−salt bath, and methylamine hydrochloride (Sigma-Aldrich, 98%, 3 g, 44 mmol) was added under stirring for 30 min. The mixture was transferred to a precooled (−20 °C) stainless steel pressure vessel and heated to 80 °C overnight. After it was cooled, the solvent was evaporated in vacuo. The product was characterized by a 70 eV mass spectrum (*m*/*z*, relative intensity): 113(3), 103(3), 102(36), 86(6), 84(3), 74(14), 73(57), 72(5), 70(13), 60(2), 59(3), 58(26), 56(3), 55(7), 45(14), 44(44), 43(36), 42(16), 41(5), 32(15), 31(17), 30(100), 29(5), 28(22), 27(5), 18(21), 17(4), 15(8). β-Alanine-N-(methyl-d_3)amide was prepared analogously using $CD_3NH_2 \cdot HCl$ (Sigma-Aldrich, 99 atom% D).

Electron impact and collisionally activated dissociation (CAD) mass spectra (collisions with air) were measured on a JEOL HX-110 double focusing mass spectrometer of EB geometry (electrostatic analyzer E precedes magnetic sector B). Ions were generated by chemical ionization[18] with NH_3/NH_4^+, acetone/$(CH_3)_2COH^+$, or acetone-d_6/$(CD_3)_2COD^+$ in an ion source that was maintained at 200−220 °C. The acetone-derived reagents add a single proton or deuteron to the analyte molecule without exchange of labile amine and amide protons.[19] For CAD, air was admitted to the first field free region at pressures to achieve 70 or 50% transmittance of the precursor ion beam at 10 keV. The CAD spectra were recorded by scanning E and B while maintaining a constant B/E ratio (B/E linked scan). The mass resolution in these linked scans was >500.

Neutralization−reionization ($^+NR^+$) mass spectra were measured on a tandem quadrupole acceleration−deceleration mass spectrometer described previously.[20] Precursor cations were generated by chemical ionization in a tight ion source maintained at 200−220 °C, passed through a quadrupole mass analyzer operated in a radiofrequency-only mode, and accelerated to 7250 eV. Alternatively, precursor ions were produced by electrospray ionization at atmospheric pressure in a special interface,[21] transported into the vacuum system by an electrodynamic funnel lens and an octopole ion guide, passed through the first quadrupole mass analyzer operated in an radiofrequency-only mode, and accelerated to 7250 eV. The fast ion beam was intercepted by dimethyldisulfide vapor (electron donor) in a collision cell floated at −7170 V at pressures to achieve 70% beam transmittance. According to Poisson statistics, out of the 30% ion fraction that underwent collisions, 83% collided only once. The interaction time for electron transfer from the donor to the fast precursor ion was estimated from the precursor ion velocity (116 520 m s^{-1} at 7250 eV) and cross-section ($\approx 1 \times 10^{-14}$ cm^2) as 1×10^{-14} s. The residual ions were reflected by an electrostatic lens floated at 250 V, and the fast neutral beam was allowed to drift to the second collision cell. The drift time, $t = 5.15$ μs, determines the width of the observation window for neutral dissociations. The dissociation products were nonselectively ionized by collisions with O_2 at 70% transmittance, and the resulting ions were decelerated to 75−80 eV kinetic energy, energy filtered, and mass analyzed by a quadrupole mass filter that was operated at unit mass resolution. Data were recorded at a scan rate of 200 points per peak, and the spectra were averaged over 50−100 scans. The ionization and NR parameters were calibrated daily with carbon disulfide when in the chemical ionization mode or protonated adenine when in the electrospray mode.[22]

Calculations. Standard ab initio calculations were performed using the Gaussian 03 suite of programs.[23] Optimized geometries were obtained by density functional theory calculations using Becke's hybrid functional (B3LYP)[24] and the 6-31++G(d,p) basis set. The optimized structures are shown in the pertinent schemes and figures. Complete optimized structures of all local minima and transition states can be obtained from the corresponding author upon request. Spin unrestricted calculations were performed for all open-shell systems. Stationary points were characterized by harmonic frequency calculations with B3LYP/6-31++G(d,p) as local minima (all real frequencies) and first-order saddle points (one imaginary frequency). The calculated frequencies were scaled with 0.963 and used to obtain zero-point energy corrections, enthalpies, and entropies. The rigid rotor harmonic oscillator (RRHO) model was used in thermochemical calculations except for low-frequency modes where the vibrational enthalpy terms that exceeded 0.5 RT were replaced by free internal rotation terms equal to 0.5 RT. It has been shown previously that enthalpies and entropies based on the RRHO and free rotation approximations bracket the more accurate values calculated with the hindered internal rotor model,[25] and the small differences cancel out in calculations of relative enthalpies and entropies.

Improved energies were obtained by single-point calculations that were carried out at several levels of theory, including split-valence triple-ζ basis sets of increasing size furnished with polarization and diffuse functions, for example, 6-311++G-(2df,p) and 6-311++G(3df,2p). For the molecular systems of the β-alanine N-methyl amide radical size, the larger basis set comprised 538 primitive gaussians. The spin-unrestricted formalism was used for calculations of open-shell systems. Contamination by higher spin states was modest, as judged from the expectation values of the spin operator $\langle S^2 \rangle$ that were ≤0.76

TABLE 1: Relative Enthalpies and Free Energies of β-Alanine N-Methyl Amide Isomers

	relative energy[a,b]					
	B3LYP	B3-MP2	B3-MP2	CCSD(T)[c]		
	6-31++G(d,p)	6-311++G(2df,p)	6-311++G(3df,2p)	6-311++G(3df,2p)		
amide	$\Delta H_{g,298}^{\circ}$	$\Delta H_{g,298}^{\circ}$	$\Delta H_{g,298}^{\circ}$	$\Delta H_{g,298}^{\circ}$	$\Delta G_{g,298}^{\circ}$	$\Delta G_{g,500}^{\circ}$
1a	0	0	0	0	0	0
1b	6.4	8.1	7.7	9.5	8.8	5.7
2a	8.6	9.1	9.3	9.2	14	16
2b	19	21	21	22	25	25

[a] In units of kilojoule per mole. [b] Including B3LYP/6-31++G(d,p) zero-point vibrational energies, enthalpies, and entropies at indicated temperatures. [c] From basis set expansion: E[CCSD(T)/6-311++G(3df,2p)] = E[CCSD(T)/6-311+G(d,p)] + E[MP2/6-311++G(3df,2p)] − E[MP2/6-311+G(d,p)].

for UB3LYP and ≤0.78 for UMP2 calculations. The UMP2 energies were corrected by spin annihilation[26] that reduced the $\langle S^2 \rangle$ to close to the theoretical value for a pure doublet state (0.75). Spin annihilation lowered the total MP2 energies by 6 millihartree (15.7 kJ mol^{-1}, root-mean-square deviation) for local energy minima and transition states. The B3LYP and MP2 energies calculated with the large basis set were combined according to the B3-MP2 scheme, as described previously.[27] Single-point energies were also calculated with coupled-cluster theory[28] including single, double, and disconnected triple excitations [CCSD(T)][29] and the 6-311+G(d,p) basis sets. These were then extrapolated to effective CCSD(T)/6-311++G(3df,-2p) using the standard formula (eq 1)

$$E[\text{CCSD(T)/large basis set}] \cong E[\text{CCSD(T)/small basis set}] + E[\text{MP2/large basis set}] - E[\text{MP2/small basis set}] \quad (1)$$

This level of theory is similar to that used in the Gaussian 2(MP2) scheme,[30] which pivots about a single-point energy calculated with the quadratic configuration interaction method [QCISD(T)][31] and the 6-311G(d,p) basis set. The use of the larger 6-311+G(d,p) basis set in the present work was motivated by the need to incorporate diffuse functions on C, N, and O in the coupled-cluster treatment of correlation energy in hypervalent ammonium radicals and transition states for their dissociations and isomerizations. Hypervalent ammonium radicals have unpaired electrons in frontier molecular orbitals that resemble atomic 3s and 3p Rydberg orbitals and show substantial diffuse character, as studied previously for simple systems.[32] Spin corrections due to the MP2 single-point energies canceled out to within 0.12 millihartree (0.3 kJ mol^{-1}) in the CCSD(T) energies calculated according to eq 1.

Excited-state energies were calculated with time-dependent density functional theory[33] using the B3LYP functional and the 6-311++G(3df,2p) basis set. Atomic spin and charge densities were calculated using the natural population analysis (NPA) method.[34]

Unimolecular rate constants were calculated according to the Rice−Ramsperger−Kassel−Marcus (RRKM) theory[35] using Hase's program[36] that was recompiled and run under Windows XP.[37] RRKM rate constants were obtained by direct count of quantum states at internal energies that were increased in 0.4 kJ mol^{-1} steps from the transition state up to 20 kJ mol^{-1} above it and then in 2 kJ mol^{-1} steps up to 350 kJ mol^{-1}. Rotations were treated adiabatically, and the calculated $k(E,J,K)$ microscopic rate constants were Boltzmann-averaged over the thermal distribution of rotational states at 473 K, corresponding to the ion source temperature, to provide canonical rate constants $k(E)$.

SCHEME 3

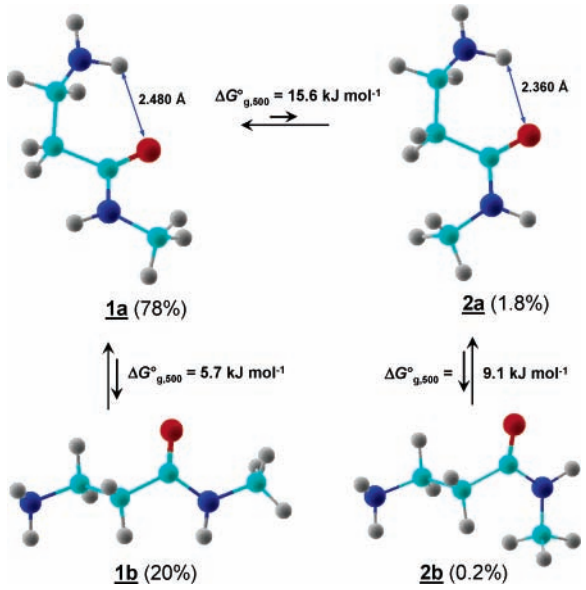

Results and Discussion

Ion Formation, Structures, and Energetics. Because of the presence of an amide group and the flexible side chain, gas-phase β-alanine N-methyl amide, its protonated forms, and radicals derived therefrom, may exist as several stable isomers differing in the amide geometry (*cis* or *trans*) and side-chain conformations. We first address the structures and energetics of neutral and protonated BANMA isomers to establish which forms are likely to be represented in the experiments described below. Table 1 shows the calculated relative enthalpies and free energies of four gas-phase BANMA isomers (**1a**, **1b**, **2a**, and **2b**; for structures, see Scheme 3).

The thermochemically most stable isomer (**1a**) is a *trans*-amide in which the side-chain amino group is hydrogen-bonded to the amide carbonyl (Scheme 3). The unfolded *trans*-amide (**1b**) was calculated to be 9.5 kJ mol^{-1} less stable than **1a** when based on 298 K enthalpies. However, **1b** has a higher entropy than **1a**, which we attribute to the lower harmonic frequencies for torsional motions of the side chain in **1b**. Consequently, the free energy difference between **1b** and **1a** is only 5.7 kJ mol^{-1} at the ion source temperature of 500 K, resulting in an equilibrium mixture consisting of 78% **1a** and 20% **1b**. The folded *cis*-amide **2a** is less stable than both **1a** and **1b** and is calculated to be populated at 1.8% at 500 K (Scheme 3).

Ions corresponding to protonated BANMA were generated by exothermic proton transfer from gas-phase NH_4^+ or $(CH_3)_2C{-}OH^+$ under conditions of chemical ionization and also by electrospray ionization from aqueous-methanol solutions. Pro-

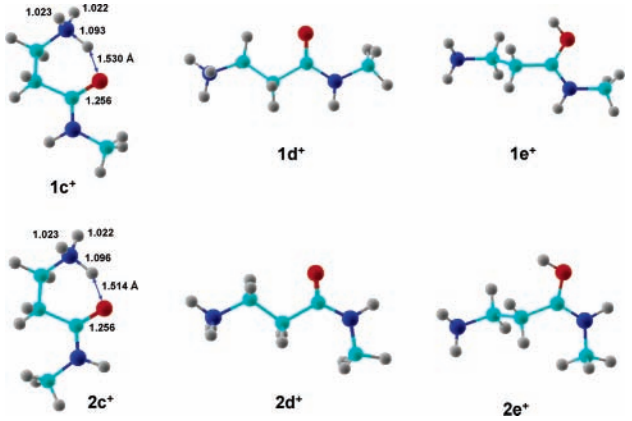

Figure 1. B3LYP/6-31++G(d,p) optimized ion structures. Bond lengths and hydrogen bonds (double arrows) are given in angstroms.

tonation in the gas phase of **1a**−**2b** can form several ion isomers differing in the protonation site and conformation. Out of those, the β-amine-protonated and internally solvated ion $\mathbf{1c}^+$ was calculated to be the most stable isomer (Figure 1 and Table 2). The proton affinity (PA) and gas-phase basicity (GB) for $\mathbf{1c}^+ \rightarrow \mathbf{1a} + H^+$ were calculated as PA(**1a**) = 971 and GB(**1a**) = 932 kJ mol^{-1} when based on CCSD(T)/6-311++G(3df,2p) energies and B3LYP/6-31++G(d,p) enthalpies and entropies. Hence, proton transfer to **1a** from NH_4^+ [PA(NH_3) = 853.5 kJ mol^{-1}] and $(CH_3)_2C{-}OH^+$ [PA(acetone) = 812 kJ mol^{-1}][38] to form $\mathbf{1c}^+$ is exothermic by 117 and 159 kJ mol^{-1}, respectively. The proton affinities and gas-phase basicities of the other isomers follow from the tabulated neutral and ion relative enthalpies and free energies (Tables 1 and 2) and are collated in Table S1 of the Supporting Information. We note that the gas-phase basicities of the related β-alanine and β-alanylglycine were reported from bracketing experiments as GB = 874 ± 5 and 905 ± 5 kJ mol^{-1}, respectively.[39]

Unfolding the side chain in $\mathbf{1c}^+$ breaks the hydrogen bonding between the ammonium and amide groups to form ion $\mathbf{1d}^+$. This side-chain unfolding is substantially endothermic destabilizing $\mathbf{1d}^+$ by 63 kJ mol^{-1} relative to the folded structure $\mathbf{1c}^+$. Protonation at the amide carbonyl in **1b** gives ion $\mathbf{1e}^+$, which is destabilized against $\mathbf{1c}^+$ by 84 kJ mol^{-1} at 298 K (Table 2). The Table 2 data further indicate that, in the absence of intramolecular hydrogen bonding, the primary amino group in **1b** is 21 kJ mol^{-1} more basic than the amide carbonyl group. We note that internal solvation of the OH group in $\mathbf{1e}^+$ by hydrogen bonding to the side-chain amino group did not result in a stable structure but led to spontaneous isomerization to $\mathbf{1c}^+$.

Protonation at the amino group in *cis*-amide **2a** gives rise to an internally solvated ion ($\mathbf{2c}^+$), which is 10 kJ mol^{-1} less stable than $\mathbf{1c}^+$ (Table 2). Unfolded ion isomers derived from *cis*-amide **2b** (ions $\mathbf{2d}^+$ and $\mathbf{2e}^+$) are both substantially less stable than $\mathbf{1c}^+$ (Table 2) and are not likely to be present at gas-phase equilibrium. The calculated free energies for $\mathbf{1c}^+$ and $\mathbf{2c}^+$ indicate 96 and 4% of these *trans*- and *cis*-ion isomers, respectively, to be present at a 500 K equilibrium under conditions typical for a chemical ionization ion source. The 298 K equilibrium, corresponding to gas-phase ions formed by electrospray, is calculated to consist of 99.2% $\mathbf{1c}^+$ and 0.8% $\mathbf{2c}^+$. We note that exothermic chain folding in $\mathbf{1d}^+$ and $\mathbf{1e}^+$ requires rotational energy barriers on the order of 10−15 kJ mol^{-1} and therefore is expected to be fast in gas-phase ions even at 298 K. Thus, the populations of the *trans*-amide conformers should be governed by the equilibrium thermodynamics favoring $\mathbf{1c}^+$. The same should hold for the *cis*-amide conformers $\mathbf{2c}^+{-}\mathbf{2e}^+$ among which $\mathbf{2c}^+$ is by far the most stable ion. The populations of the folded conformers $\mathbf{1c}^+$ and $\mathbf{2c}^+$ are governed by their relative free energies if they reach equilibrium at the ion source temperature or by the populations of neutral amides **1a** and **2a** if the ions do not equilibrate upon or following protonation. In either case, and regardless of the mode of ionization, the internally solvated *trans*-isomer $\mathbf{1c}^+$ is predicted to be the dominating ion species in the gas phase.

Ion Dissociations. Although ion dissociations were not the primary subject of this study, they play a role in the processes forming the species that are observed in the neutralization−reionization mass spectra. First, collisional electron transfer occurs collaterally with collision-induced dissociation of precursor ions, and the neutral fragments from ion dissociations are mixed with products of dissociations occurring after collisional neutralization. Although collision-induced dissociations are, in general, diminished relative to electron transfer when polarizable organic molecules such as dimethyldisulfide are used as targets, they cannot be completely suppressed, either. Second, collisional reionization with O_2 results in excitation and fragmentation of a fraction of the ions formed, so that the $^+NR^+$ mass spectra also contain products of ion dissociations occurring after the reionization step. The products of ion dissociations can usually be disentangled from those of neutral dissociations by monitoring CAD mass spectra of the precursor ion and other reference species.

CAD at 10 keV kinetic energy of $\mathbf{1c}^+$ (*m*/*z* 103) resulted in the formation of fragment ions at *m*/*z* 102 (loss of H), *m*/*z* 86 (loss of NH_3), *m*/*z* 74−72 (loss of $CH_3{-}5N$), *m*/*z* 70 (loss of $CH_3NH_2 + H_2$), *m*/*z* 58 $(CONHCH_3)^+$, *m*/*z* 45 $(^\bullet CH_2CH_2NH_3)^+$, *m*/*z* 32 $(CH_3NH_3)^+$, and *m*/*z* 30 $(CH_2{=}NH_2)^+$ (Figure 2a). Note that the CAD spectra of $\mathbf{1c}^+$ prepared by ionization with NH_4^+ and $(CH_3)_2COH^+$ were very similar and showed only minor differences in the relative intensities of fragments at *m*/*z* 73, 72, 32, and 30 (Figure 2b). The fragment ion assignments were aided by the analysis of CAD spectra of deuterium-labeled ions $\mathbf{1c}^+$-d_1 and **1c**-d_3^+, which showed the corresponding mass shifts (Figure 2c,d, also shown are the precursor ion structures). For example, the loss of ammonia involved mainly the hydrogen atoms of the side-chain ammonium group, as evidenced by the prominent loss of NH_2D from $\mathbf{1c}^+$-d_1. The structure of the (**1c** - NH_3)$^+$ ion has not been further elucidated. The *m*/*z* 58 peak was shifted to *m*/*z* 61 in the CAD spectrum of $\mathbf{1c}^+$-d_3 (Figure 2d) indicating retention of the amide CD_3 group. The loss of $CH_2{=}NH$ (*m*/*z* 74) and the formation of $CH_2{=}NH_2^+$ (*m*/*z* 30) involved mainly the side chain $-CH_2NH_2$ group, as evidenced by the mass shift of *m*/*z* 74 to *m*/*z* 77 and no shift for *m*/*z* 30 in the CAD spectrum of $\mathbf{1c}^+$-d_3. In contrast, the $CH_3NH_3^+$ ion did originate from the amide $HNCH_3$ group, as evidenced by the mass shift to *m*/*z* 35 in the CAD spectrum of $\mathbf{1c}^+$-d_3. At least one of the protons transferred to the $CH_3NH_3^+$ fragment originated from the side-chain ammonium group, as evidenced by the mass shift to *m*/*z* 33 in the CAD spectrum of $\mathbf{1c}^+$-d_1. The ion dissociations are summarized and visualized in Scheme 4, which also shows in bold characters the neutral fragments that may potentially appear in the $^+NR^+$ mass spectra.

Radical Dissociations. Collisional neutralization followed by reionization resulted in substantial dissociation so that the $^+NR^+$ mass spectra did not show any peaks at *m*/*z* 103 due to reionized $\mathbf{1c}^\bullet$ (survivor ions). The $^+NR^+$ mass spectra of $\mathbf{1c}^+$ prepared by $(CH_3)_2C{-}OH^+$ and NH_4^+ protonation and by electrospray ionization were practically identical, and thus, only the former is shown here (Figure 3a). The other $^+NR^+$ mass spectra are given in Figures S1 and S2 of the Supporting Information. The $^+NR^+$ spectrum showed major fragments at *m*/*z* 28 and *m*/*z* 42

TABLE 2: Relative Enthalpies and Free Energies of β-Alanine N-Methyl Amide Cations

	relative energy[a,b]					
	B3LYP	B3-MP2	B3-MP2	CCSD(T)[c]		
	6-31++G(d,p)	6-311++G(2df,p)	6-311++G(3df,2p)	6-311++G(3df,2p)		
ion	$\Delta H_{g,298}^{\circ}$	$\Delta H_{g,298}^{\circ}$	$\Delta H_{g,298}^{\circ}$	$\Delta H_{g,298}^{\circ}$	$\Delta G_{g,298}^{\circ}$	$\Delta G_{g,500}^{\circ}$
1c$^+$	0	0	0	0	0	0
1d$^+$	66	65	64	63	57	52
1e$^+$	86	86	84	84	78	72
2c$^+$	9.8	10.0	10.1	10.1	12.0	13.3
2d$^+$	74	72	72	70	65	61
2e$^+$	94	95	92	92	88	83

[a] In units of kilojoule per mole. [b] Including B3LYP/6-31++G(d,p) zero-point vibrational energies, enthalpies, and entropies at indicated temperatures. [c] From basis set expansion: E[CCSD(T)/6-311++G(3df,2p)] = E[CCSD(T)/6-311+G(d,p)] + E[MP2/6-311++G(3df,2p)] − E[MP2/6-311+G(d,p)].

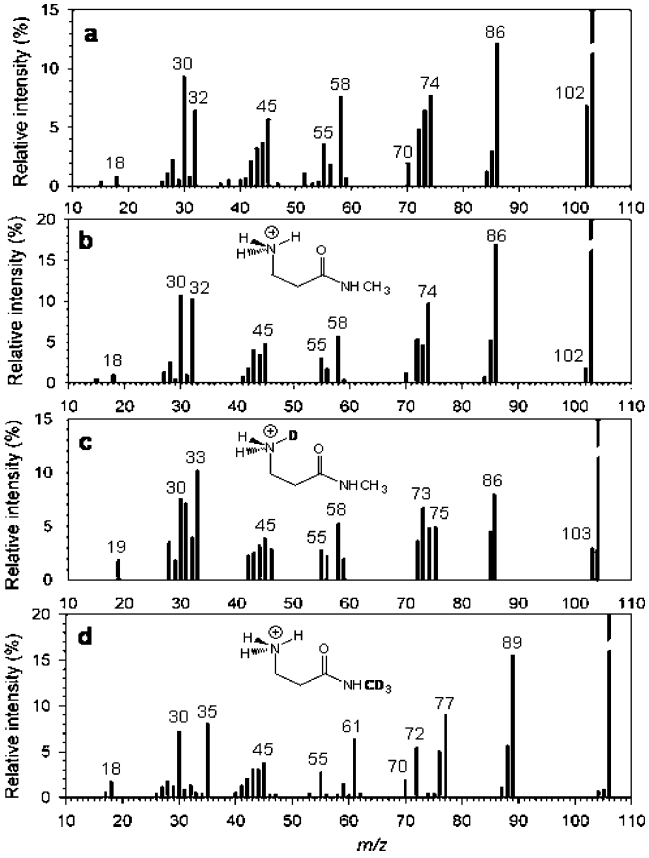

Figure 2. CAD mass spectra (10 keV) of (a) ion **1c**$^+$ by NH_3/NH_4^+ chemical ionization, (b) **1c**$^+$ by acetone/$(CH_3)_2C-OH^+$ chemical ionization, (c) ion **1c**$^+$-d_1 by acetone/$(CD_3)_2C-OD^+$ chemical ionization, and (d) **1c**$^+$-d_3 by by NH_3/NH_4^+ chemical ionization.

that were identified as CO and CH_2CO, respectively. This assignment was based on the absence of mass shift for *m*/*z* 28 and 42 in the $^+NR^+$ mass spectra of deuterium-labeled ions **1c**-d_1^+ (Figure 3b), **1c**$^+$-d_3, and **1c**$^+$-d_4 (Figures S3 and S4, Supporting Information). The *m*/*z* 30 fragment was identified as CH_2NH_2 originating from the alanine side chain, as corroborated by the peaks at *m*/*z* 30 and 32 in the $^+NR^+$ mass spectra of **1c**$^+$-d_3 and **1c**$^+$-d_4, respectively. Note that dissociations of **1c**$^{\bullet}$-d_1 produced both CH_2NH_2 at *m*/*z* 30 and CH_2NHD at *m*/*z* 31. The *m*/*z* 31 fragment from **1c**$^{\bullet}$ corresponded to CH_3-NH_2 originating from the amide $HNCH_3$ group that underwent mass shifts to *m*/*z* 32 and 34 in the $^+NR^+$ mass spectra of **1c**$^+$-d_1. and **1c**$^+$-d_3, respectively. The presence and absence of mass shifts due to deuterium allowed us to identify the *m*/*z* 43 fragment as mainly HN═C═O. The *m*/*z* 55−58 group of fragments showed no mass shifts in the spectrum of **1c**$^+$-d_1 (Figure 3b), but their intensity was too low in the $^+NR^+$ mass spectra of the other labeled ions to allow for firm assignment. The fragments at *m*/*z* 70 and 73 showed partial shifts to *m*/*z* 71 and 74, respectively, in the $^+NR^+$ mass spectrum of **1c**$^+$-d_1. We also note that the NH_3 fragment (*m*/*z* 17) from **1c**$^{\bullet}$ underwent the expected mass shift to *m*/*z* 18 (NH_2D) when produced from **1c**$^{\bullet}$-d_1 (Figure 3b).

SCHEME 4

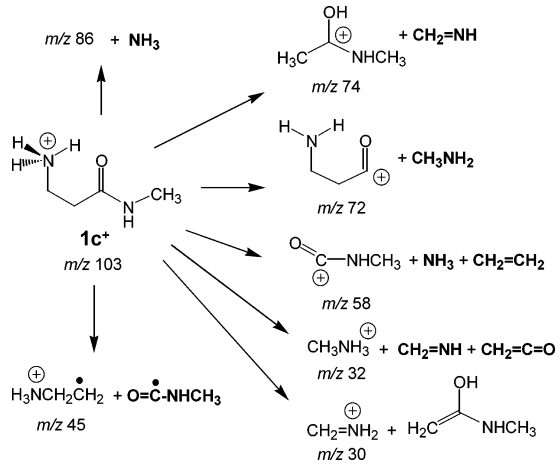

Reference spectra were obtained for potential dissociation products of radical **1c**$^{\bullet}$, for example, β-alanine N-methylamide **1a** by loss of ammonium H and N-methylacetamide enol (**3**) by intramolecular hydrogen transfer followed by cleavage of the $C_\alpha-C_\beta$ bond (see below). Product **1a** was characterized by its electron impact mass spectrum (Figure 4a). The spectrum showed a molecular ion at *m*/*z* 102 and major fragments at *m*/*z* 73, 70, 58, 43, 30, 18, and 15. With the exception of *m*/*z* 102, the same fragments appeared in the $^+NR^+$ mass spectrum of **1c**$^+$ (Figure 3a). Fragment **3** was generated by dissociative ionization of N-methylvaleramide and characterized by its $^+NR^+$ mass spectrum, which showed ions at *m*/*z* 73, 58, 43, 42, 31, 30, 28, 18, and 15 (Figure 4b). Again, all of these fragments appeared in the $^+NR^+$ mass spectrum of **1c**$^+$. Thus, it was difficult to unambiguously distinguish the dissociation pathways in **1c**$^{\bullet}$ even with the help of reference spectra and deuterium labeling. On the basis of the fragments observed in the $^+NR^+$ mass spectrum of **1c**$^{\bullet}$, we considered three plausible dissociation pathways shown in Scheme 5: (i) loss of an ammonium hydrogen atom, (ii) ammonium hydrogen atom migration onto the amide carbonyl followed by $C_\alpha-C_\beta$ or $N-CH_3$ bond cleavage, and (iii) loss of ammonia. The potential energy surface along these pathways and the dissociation kinetics were further analyzed by ab initio and RRKM calculations, as described next.

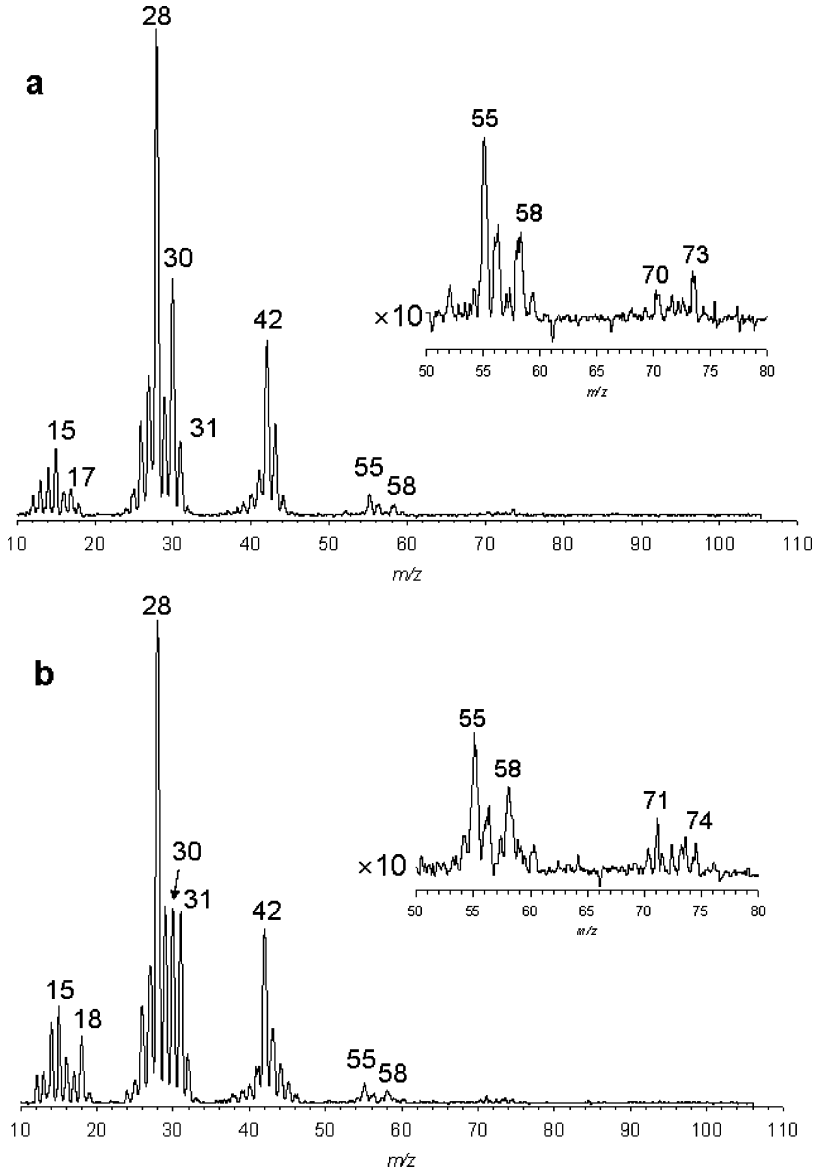

Figure 3. Neutralization (CH_3SSCH_3, 70% transmittance)/reionization (O_2, 70% transmittance) mass spectra of (a) **1c**$^+$ and (b) **1c**-d_1^+.

Radical Energetics. We first address the formation of **1c**$^\bullet$ by electron transfer and the structures and relative energies of radicals pertinent to **1c**$^\bullet$ and its isomers. Electron transfer to **1c**$^+$ results in molecular geometry changes in the radical formed (**1c**$^\bullet$; Figure 5). Most notably, the hydrogen bond to the amide group stretches from 1.530 Å in **1c**$^+$ to 1.924 Å in relaxed **1c**$^\bullet$, indicating a weaker intramolecular H-bonding in the radical. Another structural change in **1c**$^\bullet$ is the elongation of the outer ammonium N−H bonds from 1.022 to 1.023 Å in **1c**$^+$ to 1.048−1.050 Å in **1c**$^\bullet$ (Figure 5). This is typical for a hypervalent ammonium group, as calculated previously for a number of organic ammonium radicals.[32] In contrast, the N−H bond of the H-bonding proton (H_1) is shortened from 1.093 Å in **1c**$^+$ to 1.041 Å in **1c**$^\bullet$. These changes reflect the charge distribution within the ammonium group in **1c**$^\bullet$, as represented by NPA atomic spin densities (Scheme 6, blue italic characters) and charges (bold black characters). The outer two ammonium hydrogen atoms (H_2 and H_3) carry 25 and 33% of the spin density, respectively, whereas H_1 carries only 4% (Scheme 6). Accordingly, H_1 has a higher atomic charge (0.42) than do H_2 (0.22) and H_3 (0.15) and in this respect resembles a proton in an ammonium cation (Scheme 6).

The relatively weak intramolecular H-bonding in **1c**$^\bullet$, as indicated by the extended H···O distance, is reflected by the comparable relative stabilities of **1c**$^\bullet$ and its unfolded isomer **1d**$^\bullet$, $\Delta H_{g,0}$(**1c**$^\bullet$ → **1d**$^\bullet$) = 2.8 kJ mol^{-1} (Table 3). Ammonium hydrogen (H_1) transfer in **1c**$^\bullet$ to the amide carbonyl is 71 kJ mol^{-1} exothermic to form the aminoketyl radical **1f**$^\bullet$. The latter shows a pyramidized ketyl carbon atom that carries 69% of the spin density. The remaining spin density is delocalized among the aminoketyl nitrogen (12%) and oxygen atoms (10%) and the suitably oriented hydrogen atoms at the flanking methylene and methyl groups (Scheme 6). The hydroxyl proton carries no spin density but shows a stronger hydrogen bonding to the amine nitrogen at 1.883 Å distance (Figure 5) as compared to that in **1c**$^\bullet$. This is also reflected by the increased endothermicity of side-chain unfolding in **1f**$^\bullet$ to form **1e**$^\bullet$, which requires 21 kJ mol^{-1} to proceed (Table 3).

The *cis*-amide isomer **2c**$^\bullet$ was calculated to be 8.6 kJ mol^{-1} less stable than **1c**$^\bullet$ (Table 3), indicating that destabilization of the *cis*-amide geometry in **2c**$^\bullet$ was similar to that in **2b** and **2d**$^+$. The *cis*-aminoketyl radicals derived from **2c**$^\bullet$, for example, **2e**$^\bullet$ and **2f**$^\bullet$, are very similar by energy to their *trans*-isomers **1e**$^\bullet$ and **1f**$^\bullet$, respectively. Because the *cis*-amide isomers of

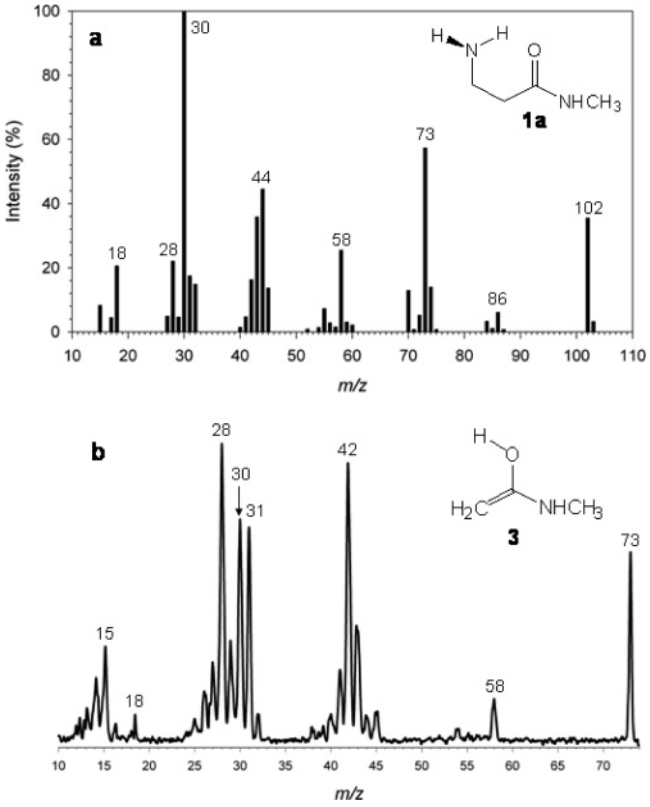

Figure 4. (a) Reference 70 eV electron ionization mass spectrum of **1a**. (b) Neutralization (CH_3SSCH_3, 70% transmittance)/reionization (O_2, 70% transmittance) mass spectrum of **3**.

SCHEME 5

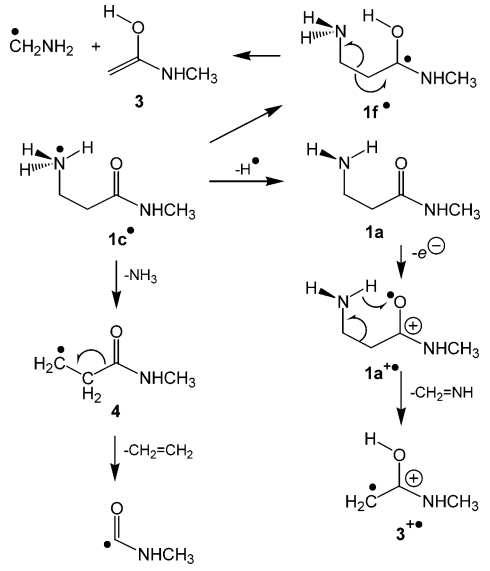

precursors and reactants (**2a**, **2c**$^+$, and **2c**$^\bullet$) are in general less populated than their *trans*-isomers, the further discussion of radical dissociation energetics and kinetics will focus on the latter.

Neutralization and Dissociation Energetics. Radical **1c**$^\bullet$ is formed by vertical electron transfer from the molecular donor to ion **1c**$^+$ that is characterized by the corresponding ionization and recombination energies. The vertical recombination energy in **1c**$^+$ was calculated by B3-PMP2 to be $RE_{vert} = 3.16$ eV. Relevant to collisional neutralization, vertical electron transfer from dimethyldisulfide ($IE_{vert} = 8.96$ eV) to **1c**$^+$ is estimated to be $8.96-3.16 = 5.8$ eV endothermic. The energy deficit is balanced by conversion of a small fraction of the available center-of-mass collision energy (3460 eV) to the internal energy of the (**1c**$^+$ + CH_3SSCH_3) system.

The adiabatic ionization energy of **1c**$^\bullet$ was calculated as $IE_{adiab} = 3.40-3.41$ eV at the B3-PMP2 levels of theory and slightly lower ($IE_{adiab} = 3.33$ eV) by effective CCSD(T)/6-311++G-(3df,2p). This indicates that the unpaired electron is only weakly bound in radical **1c**$^\bullet$. The electron binding in **1c**$^\bullet$ was found to be even weaker than in other hypervalent aliphatic ammonium radicals, for example, methylammonium and ethylammonium, where $IE_{adiab} = 4.24$ and 4.08 eV, respectively,[32d] and also weaker than in the unfolded radical **1d**$^\bullet$, which has $IE_{adiab} = 3.95$ eV. The very low IE_{adiab} of **1c**$^\bullet$ can be in part attributed to the substantial stabilization by intramolecular H-bonding of ion **1c**$^+$ (63 kJ mol^{-1}, Table 2) as compared to that in **1c**$^\bullet$ (2.8 kJ mol^{-1}, Table 3).

The difference between the adiabatic ionization energy of **1c**$^\bullet$ and the recombination energy in **1c**$^+$, $E_{FC} = 24$ kJ mol^{-1}, provides an estimate of the vibrational excitation due to Franck−Condon effects in **1c**$^\bullet$ formed by vertical electron transfer to the ground doublet electronic state [$X(^2A)$]. The internal energy of radicals **1c**$^\bullet$ in the $X(^2A)$ state was estimated as a sum of the Franck−Condon energy and the mean enthalpy of the precursor ion,[40] $\langle E\rangle = E_{FC} + E_{ion}$. The E_{ion} term was bracketed between the rovibrational enthalpy of the precursor ion **1c**$^+$ at the ion source temperature (500 K, 42 kJ mol^{-1}) as a lower bound and the energy gained upon proton transfer as an upper bound. For the latter, we took the fraction of the protonation exothermicity that was equipartitioned between the **1c**$^+$ and the conjugate base of the protonation reagent at 500 K, which gave $E_{ion} = 110$ and 112 kJ mol^{-1} for proton transfer from $(CH_3)_2C-OH^+$ and NH_4^+, respectively. The combined E_{FC} and E_{ion} gave a range of mean internal energies in **1c**$^\bullet$ to be $\langle E\rangle = 66-136$ kJ mol^{-1}. When radical **1c**$^\bullet$ was produced by electrospray ionization at 298 K followed by electron transfer, its estimated internal energy was $\langle E\rangle = E_{FC} + E_{ion} = 24 + 16 = 40$ kJ mol^{-1}. The $^+NR^+$ mass spectra indicate that within these limits the radical internal energy had no major effect on the dissociations.

The adiabatic ionization energy of the aminoketyl radical **1f**$^\bullet$ could not be calculated because the corresponding ion (**1f**$^+$) is intrinsically unstable and isomerizes by proton transfer to **1c**$^+$. The adiabatic ionization energy of the unfolded aminoketyl radical (**1e**$^\bullet$) was calculated as $IE_{adiab} = 4.71$ eV (CCSD(T) value).

As indicated by the Table 3 data, radical **1c**$^\bullet$ is metastable with respect to the exothermic isomerization to the aminoketyl radical **1f**$^\bullet$. The dissociation energies of **1c**$^\bullet$ and the relevant transition state energies are summarized in Table 4. The energies from extrapolated CCSD(T)/6-311++G(3df,2p) calculations are discussed in the text. Loss of an ammonium hydrogen atom was calculated to be 27 kJ mol^{-1} exothermic when forming the most stable amide **1a**. The N−H bond dissociation proceeded through a transition state (TS1) that was located at $d(N-H) = 1.401$ Å (Figure 6). Simultaneously with elongating the dissociating N−H bond, the hydrogen bond of the bridging proton is elongated to 2.139 Å in TS1 to eventually reach 2.480 Å in the product **1a**. TS1 was calculated to be only 12 kJ mol^{-1} above **1c**$^\bullet$, indicating a facile dissociation by ammonium H loss.

The potential energy surface along the N−H dissociation coordinate between **1c**$^\bullet$ and TS1 is comparably well-represented by both B3LYP and PMP2 calculations that show similar energy barriers (Figure 7a). However, past TS1, the B3LYP calculations show a false potential energy minimum around $d(N-H) = 2.0$ Å, which is not reproduced by PMP2 single-energy calculations.

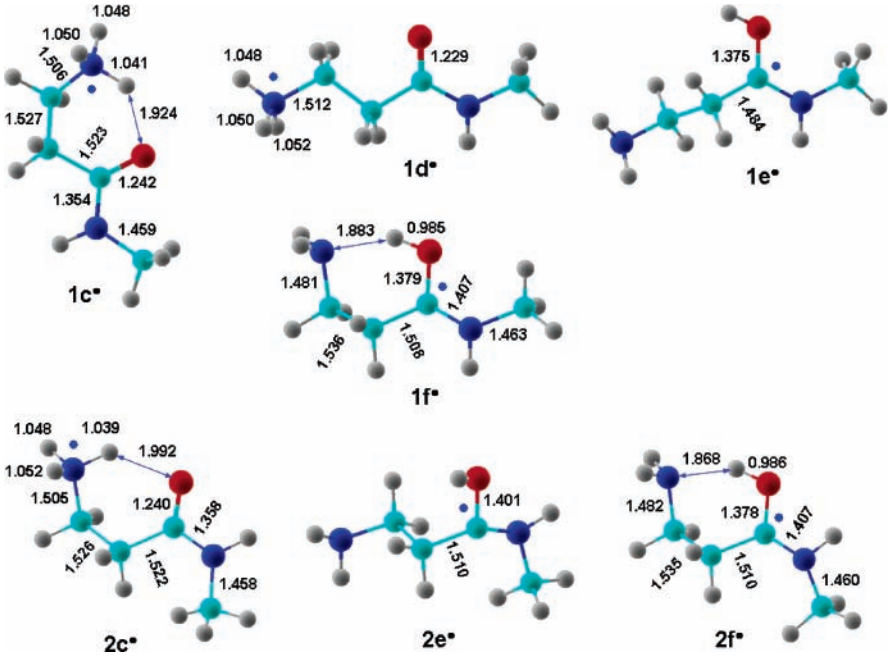

Figure 5. B3LYP/6-31++G(d,p) optimized structures of radicals. Bond lengths and hydrogen bonds (double arrows) are given in angstroms.

SCHEME 6

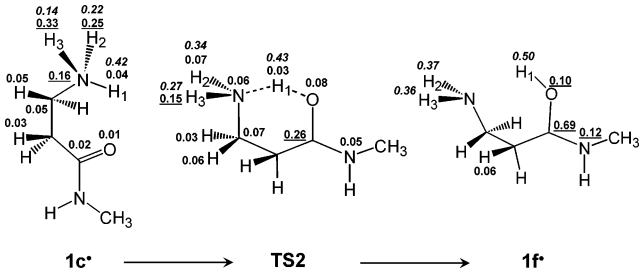

After the B3-PMP2 correction, the potential energy shows a smoothly descending surface that converges to the products (**1a** + H). Note that both the TS1 and the product relative energy are very well-represented by B3-PMP2 when compared to the same energies from extrapolated CCSD(T) calculations (Table 4).

The competing transfer of the bridging ammonium hydrogen atom to the amide carbonyl showed a complicated potential energy surface that was investigated in some detail. The B3LYP potential energy surface along the reaction path showed a well-developed transition state at d(N−H) = 1.139 Å and d(H−O) = 1.414 Å (TS2, Figure 7b). TS2 is an early transition state, consistent with the substantially exothermic isomerization of **1c•** to **1f•** (Table 3). The B3LYP TS2 energies were only 3−4 kJ mol^{-1} above **1c•** when calculated with the three basis sets used here and corrected for zero-point vibrational energies (Table 4). However, PMP2 single-point energies showed a cusp at the TS2 geometry and in its close vicinity (Figure 7b). A cusp at the TS2 geometry was also found for single-point CCSD(T) energies. Unfortunately, the cusp distorts both the PMP2 and the B3-PMP2 potential energy surfaces and thus makes it impossible for one to use single-point TS calculations for an accurate representation of TS2 energy. Instead of using a single-point TS energy, we resorted to interpolation whereby the potential energy surface along the H-migration coordinate was mapped with single-point CCSD(T) calculations in the vicinity of TS2 geometry (Figure 7b). Excluding TS2, the single-point energies at six points between d(H−O) = 1.35 and 1.55 Å showed a smooth surface that was least-squares fitted with a quadratic function that exhibited a maximum at d(H−O) = 1.480 Å. The parabolic fit was acceptably tight, giving a root-mean square deviation of only 0.6 kJ mol^{-1} from the single-point CCSD(T) energies. The maximum of the fitted curve was corrected for zero-point energies and thus-obtained TS2 energy (8.6 kJ mol^{-1} relative to **1c•**, Table 4) was used as our best guess for RRKM calculations (see below). The probable reason for the occurrence of the cusp on the potential energy surface is addressed later in the paper.

Another potentially competing dissociation of **1c•** involved nearly thermoneutral unfolding of the side chain to **1d•**, followed by loss of ammonia to form radical **4**. This was found to be the most exothermic dissociation of **1c•** at $\Delta H_{rxn}^{\circ} = -102$ kJ mol^{-1} (Table 4). However, reaching the transition state for the H_3N-C bond cleavage in **1d•** (TS7) required a relatively high energy, which made it noncompetitive with H loss and migration in **1c•**.

The highly exothermic isomerization of **1c•** to **1f•** raised the question of consecutive dissociations of this aminoketyl radical intermediate. The unpaired electron in radical **1f•** (Scheme 6) was presumed to activate the adjacent C−C, N−C, C−H, N−H, and O−H bonds for β-fission type of dissociations; hence, transition states for cleavages of the $C_\alpha-C_\beta$ and $N-C_\alpha$ bonds were selected for investigation. The former dissociation proceeds through TS6 to form enolimine **3** and a CH_2NH_2 radical. However, TS6 was found to have a high energy, and thus, the $C_\alpha-C_\beta$ dissociation can be expected to be slow in competition with the other dissociations of **1f•**. Loss of methyl by $N-C_\alpha$ bonds cleavage can proceed by two pathways. The less favorable of these is a direct cleavage in **1f•** that requires 104 kJ mol^{-1} in TS4. The products are a methyl radical and enolimine **5**. The more favorable pathway involves a rotation of the methylamino group in **1f•** to form the *cis*-isomer **2f•**, which is virtually isoenergetic with **1f•**. The rotation barrier for **1f•** → **2f•** is miniscule (Table 4), indicating a facile interconversion. Radical **2f•** can undergo $N-C_\alpha$ bond dissociation through TS5 at 95 kJ mol^{-1} to form a methyl radical and enolimine **6**. The difference in the TS energies between TS4 and TS5 probably reflects the different stability of the forming enolimine group. The latter prefers a *syn*-geometry, as in **6** and TS5, which has a more

TABLE 3: Relative Energies of Radicals

	relative energy[a,b]			
	B3LYP	B3-MP2	B3-MP2	CCSD(T)[c]
radical	6-31++G(d,p)	6-311++G(2df,p)	6-311++G(3df,2p)	6-311++G(3df,2p)
1c•	0	0	0	0
1d•	3.6	2.0	2.3	2.8
1e•	−35	−38	−40	−50
1f•	−58	−60	−61	−71
2c•	9.9	9.2	9.4	8.6
2e•	−34	−37	−39	−49
2f•	−59	−60	−61	−70

[a] In units of kilojoule per mole. [b] Including B3LYP/6-31++G(d,p) zero-point vibrational energies and referring to 0 K. [c] From basis set expansion: E[CCSD(T)/6-311++G(3df,2p)] = E[CCSD(T)/6-311+G(d,p)] + E[MP2/6-311++G(3df,2p)] − E[MP2/6-311+G(d,p)].

TABLE 4: Radical Dissociation and Transition State Energies

	relative energy[a,b]			
	B3LYP	B3-MP2	B3-MP2	CCSD(T)[c]
reaction	6-31++G(d,p)	6-311++G(2df,p)	6-311++G(3df,2p)	6-311++G(3df,2p)
1c• → **1a** + H•	−2	−25	−23	−27
1c• → **3** + CH_2NH_2•	12	12	10	19
1c → **4** + NH_3	−103	−106	−108	−102
1c → **5** + CH_3•	−24	−30	−31	−34
1c• → **6** + CH_3•	−41	−45	−45	−47
1c• → TS1 → **1a** + H•	13	11	12	12
1c• → TS2 → **1f•**	3.4	(18)[d]	(18)[d]	8.6[e] (17)[d]
1c• → TS3 → **1c•**	12	12	12	13
1f• → TS4 → **5** + CH_3•	91	95	96	104
2f• → TS5 → **6** + CH_3•	81	85	86	95
1f• → TS6 → **3** + CH_2NH_2•	113	116	117	133
1d• → TS7 → **4•** + NH_3	35	47	47	53
1f• → TS8 → **2f•**	10	11	11	12
2c• → TS9 → **1f•**	0.7	13	15	15

[a] In units of kilojoule per mole. [b] Including B3LYP/6-31++G(d,p) zero-point vibrational energies and referring to 0 K. [c] From basis set expansion: E[CCSD(T)/6-311++G(3df,2p)] = E[CCSD(T)/6-311+G(d,p)] + E[MP2/6-311++G(3df,2p)] − E[MP2/6-311+G(d,p)]. [d] These TS energies are adversely affected by a cusp on the PMP2 potential energy surface. [e] From a quadratic fit of the CCSD(T) potential energy surface.

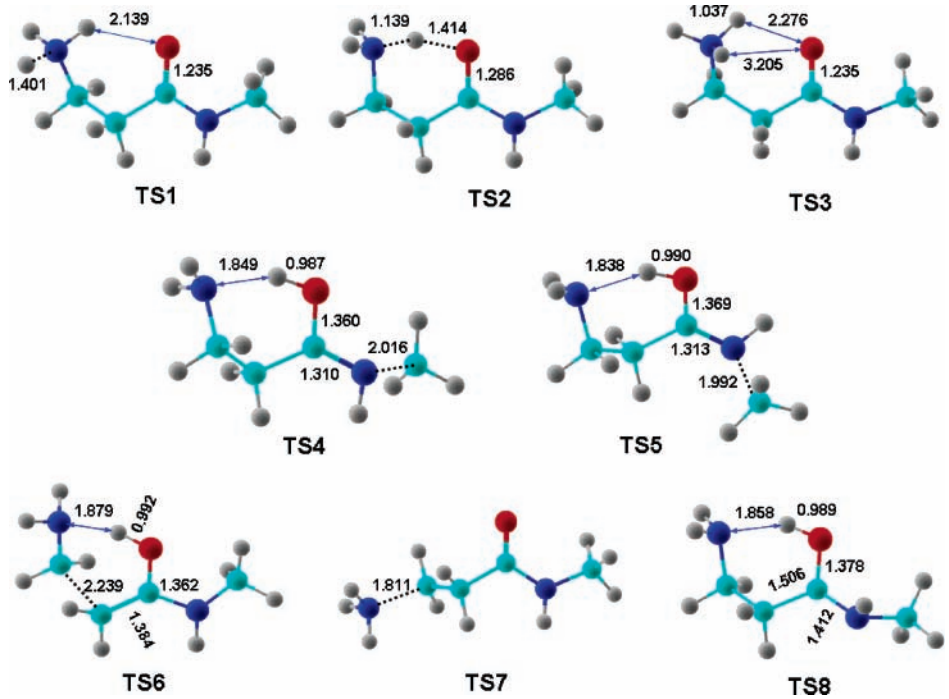

Figure 6. B3LYP/6-31++G(d,p) optimized structures of radical transition states.

favorable arrangement of the O−H and N−H bond dipoles than the *anti*-geometry in **5** and TS4. Note that both TS4 and TS5 preserve the intramolecular H-bonding of the hydroxyl and amino groups (Figure 6).

To connect the dissociations of **1c•** with those of its intermediates, the relevant parts of the potential energy surface along the dissociation pathways were plotted relative to **1c•** (Figure 8). The potential energy diagram suggests that **1c•** may

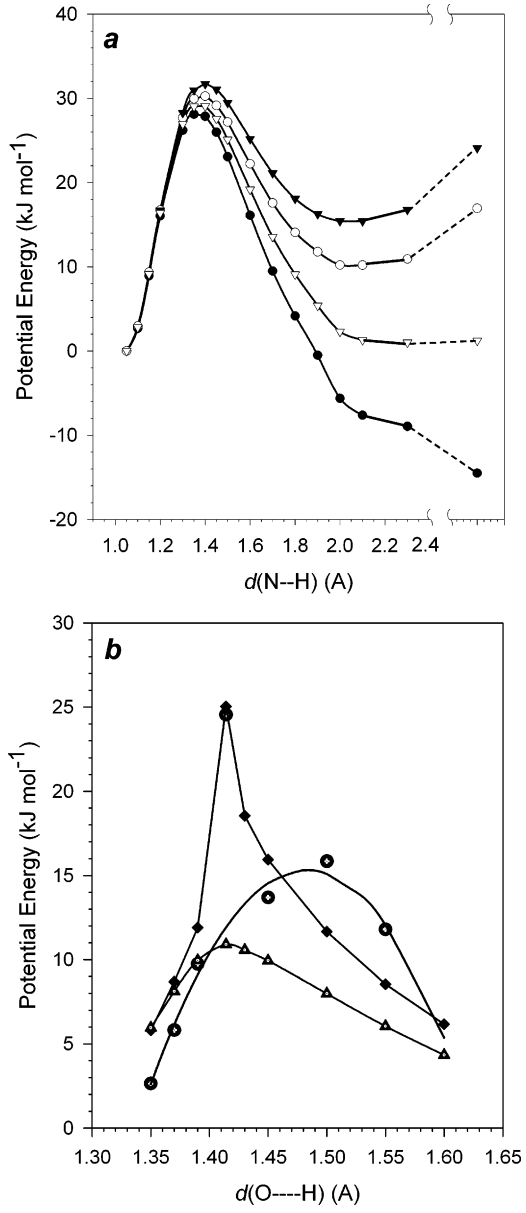

Figure 7. Potential energy surfaces along the N···H (a) and N···H···O (b) reaction coordinates in **1c•**. Top panel (a): Full triangles, B3LYP/6-31++G(d,p); open circles, B3LYP/6-311++G(2df,p); open triangles, B3-PMP2/6-311++G(2df,p); and full circles, PMP2/6-311++G(2df,p). Bottom panel (b): Open triangles, B3LYP/6-31++G(d,p); full diamonds, B3-PMP2/6-311++G(3df,2p); and open circles, CCSD(T)/6-311++G(3df,2p).

undergo competitive loss of an ammonium hydrogen atom, reversible chain unfolding to **1d•**, and exothermic isomerization to **1f•** and **2f•**. Further dissociations of **1f•** and **2f•** can be expected to compete with reversible isomerization to **1c•** and **2c•**. The kinetics of these unimolecular reactions are addressed next.

Radical Dissociation Kinetics. The extrapolated CCSD(T)/6-311++G(3df,2p) transition state energies were used for calculations of unimolecular rate constants for the reactions of interest. Figure 9a shows the rate constants (log k, s^{-1}) as functions of internal energy for dissociations and isomerizations of **1c•** by loss of ammonium hydrogen atom through TS1 (k_1), H-atom migration through TS2 (k_2), rotation of the NH_3 group through TS3 (k_3), and for loss of ammonia from radical **1d•** through TS7 (k_4). All of these rate constants were found to be greater than 10^6 s^{-1} in the 66−136 kJ mol^{-1} interval of internal energies pertinent to **1c•** when formed by vertical electron transfer. Note that $k_1-k_3 \gg 10^6$ s^{-1} also for internal energies around 40 kJ mol^{-1} that are presumed for less energetic **1c•** produced by electrospray and neutralization. This is consistent with the absence of survivor **1c•** on the experimental time scale of 5.15 μs in all $^+NR^+$ mass spectra. The H-atom migration has the lowest onset, and thus, k_2 dominates in a narrow energy interval between 8.6 and 18 kJ mol^{-1} (Figure 9b). However, k_1 shows a steep increase with internal energy, such that the curves for k_1 and k_2 cross at $E = 18$ kJ mol^{-1}, and at internal energies > 48 kJ mol^{-1}, the loss of H becomes >10-fold faster than H-atom migration. In particular, in the 66−136 kJ mol^{-1} energy interval, which is presumed for **1c•**, the loss of H is calculated to be 15−32 times faster than the H-atom migration. Interestingly, k_1 is also consistently greater than the rotation rate constant k_3 (Figure 9b). This indicates that the loss of the diastereotopic hydrogen atoms from the ammonium group is largely determined by their orientation in the reactant **1c•** and hence in the precursor ion $\mathbf{1c}^+$. The loss of ammonia (k_4) is several orders of magnitude slower than the loss of H over the entire energy interval and is not expected to be kinetically important.

Further unimolecular rate constants were calculated for isomerizations and dissociations of aminoketyl radical **1f•**, for example, for the reverse H-atom migration reforming **1c•** (k_5), N−C_α bond cleavage (k_6), C_α−C_β bond cleavage (k_7), and reversible *trans*−*cis* isomerization by rotation about the C−N bond to form **2f•** (k_8). Rate constants were also obtained for the N−C_α bond cleavage (k_9) and reverse C−N bond rotation (k_{-8}) in the *cis*-rotamer **2f•** (Figure 10). The rate constants in Figure 10 are plotted as log k on an energy scale referring to **1c•**, which is the same as in Figure 9, so the two sets of kinetic data can be directly compared. Accordingly, the internal energy of **1f•** is obtained by adding $\Delta E(\mathbf{1f^\bullet} \rightarrow \mathbf{1c^\bullet}) = 71$ kJ mol^{-1} to the energy scale in Figure 10.

The data show that the aminoketyl radicals **1f•** and **2f•** can interconvert rapidly by rotation, with k_8, $k_{-8} > 10^{11}$ s^{-1} within the entire range of internal energies pertinent to **1f•** when formed from **1c•**. The **2f•**/**1f•** ratio was calculated as $k_8/k_{-8} = 1.02-1.06$ over the energy interval shown in Figure 10, indicating that both aminoketyl radicals are comparably populated in the mixture and can serve as intermediates for further dissociation. The reverse H-atom migration (k_5) is a fast reaction in **1f•** at internal energies above 28 + 71 = 99 kJ mol^{-1}. At energies above 116 + 71 = 187 kJ mol^{-1}, the isomerization is outcompeted by methyl loss from **2f•** that may represent a viable dissociation channel. In contrast, the C_α−C_β bond cleavage was too slow to be observed (log $k_7 < 5.29$) in **1f•** produced from **1c•** possessing energies in the critical 66−136 kJ mol^{-1} interval (Figure 10).

Dissociation pathways were also considered that proceeded via the unfolded aminoketyl radicals, for example, the O−H and N−CH_3 bond cleavages in **1e•** and **2e•**. The corresponding transition states in general required higher energies than those for TS1, TS4, and TS5 and were considered kinetically less significant. The relevant transition states (TS10−TS14) are given in Table S2 and Schemes S1 and S2 of the Supporting Information. The reason for the increased TS energies for dissociations starting from **1e•** and **2e•** was probably the absence of stabilization by intramolecular hydrogen bonding.

Analysis of the kinetic data presented in Figures 9 and 10 allows us to arrive at the following conclusions. At internal energies above 18 kJ mol^{-1} and particularly in the critical 66−136 kJ mol^{-1} interval, dissociations in **1c•** favor H-atom loss over isomerization to **1f•**/**2f•**. This implies that these intermedi-

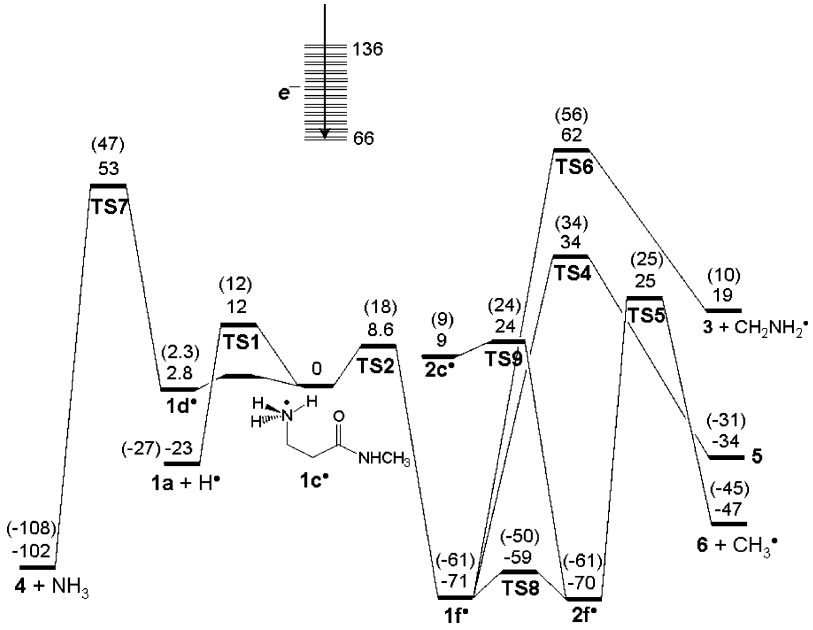

Figure 8. Overall potential energy diagram for dissociations of **1c•**. Relative energies in kJ mol^{-1} are from extrapolated CCSD(T)/6-311++G-(3df,2p) single-point calculations including B3LYP/6-31++G(d,p) zero-point energies. Energies in parentheses are from B3-PMP2/6-311++G-(3df,2p) single-point calculations and include zero-point corrections.

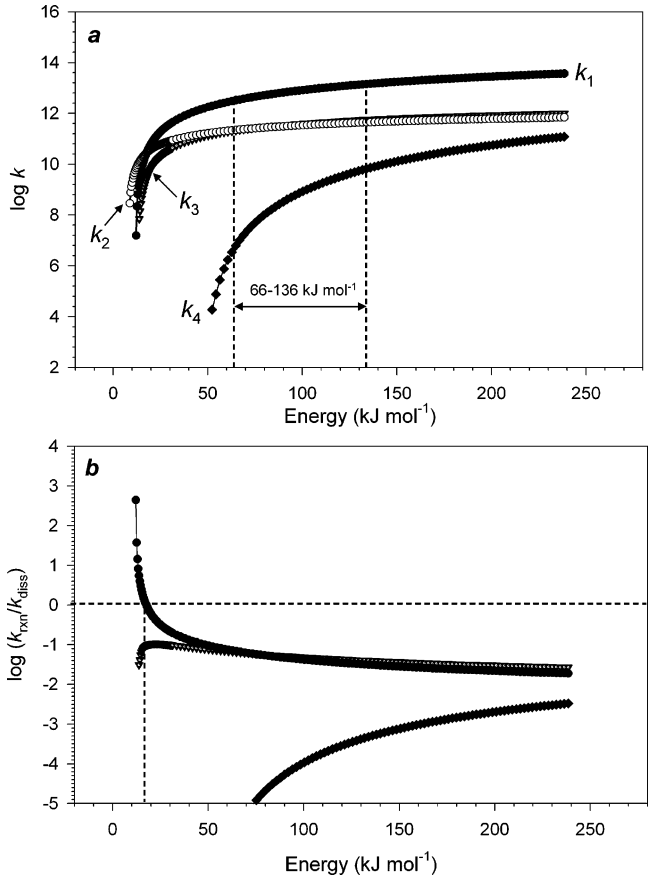

Figure 9. (a) RRKM rate constants (log k, s^{-1}) for dissociations and isomerizations of **1c•** on the extrapolated CCSD(T)/6-311++G(3df,-2p) potential energy surface of the ground electronic state. Full circles, loss of H (k_1); open circles, H migration forming **1f•** (k_2); upside triangles, NH_3 rotation (k_3); and diamonds, loss of ammonia through **1d•** (k_4). (b) Rate constants (log) relative to k_1. Full circles, log(k_2/k_1); upside triangles, log(k_3/k_1); and diamonds, log(k_4/k_1). The vertical dashed line was drawn at 18 kJ mol^{-1} indicating the crossing of the k_1 and k_2 curves.

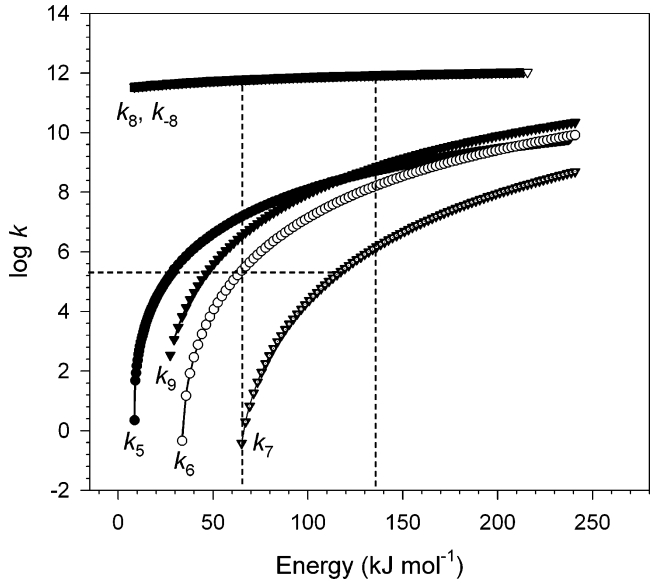

Figure 10. RRKM rate constants (log k) for dissociations and isomerizations of **1f•** on the CCSD(T)/6-311++G(3df,2p) potential energy surface of the ground electronic state. The energy scale is relative to **1c•**. Full circles, isomerization to **1c•** (k_5); open circles, N−CH_3 dissociation in **1f•** (k_6); upside open triangles, C_α−C_β bond dissociation in **1f•** (k_7); squares, **1f•** → **2f•** (k_8) and **2f•** → **1f•** (k_{-8}) isomerizations; and upside full triangles, N−CH_3 dissociation in **2f•** (k_9). The log k curve for **2f•** → **1f•** isomerization (k_{-8}) overlaps with that for k_8. The horizontal dashed line was drawn at log k = 5.29 = log(1/τ), corresponding to the experimental time scale (τ = 5.15 μs) for radical dissociations.

ates are not formed efficiently on the potential energy surface of the ground electronic state. However, high energies are needed to promote the N−C_α and C_α−C_β bond dissociations in **1f•** and **2f•**. Hence, the only kinetically plausible way for the latter dissociations to occur is to produce **1f•** and **2f•** with sufficiently high internal energies while avoiding the competing loss of H. This may be possible by starting from an excited electronic state of **1c•**, because ammonium radicals are known to be strongly bound along the N−H coordinates in excited states.[5,32c]

Excited Electronic States. Vertical electron capture in **1c**$^+$ can occur to place the electron in any of the available bound

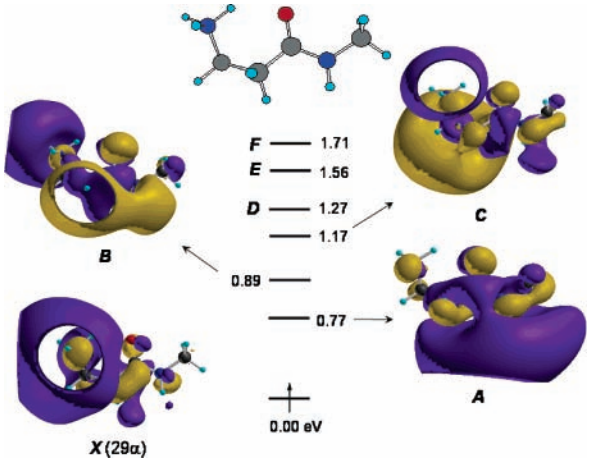

Figure 11. Molecular orbitals for excited electronic states in **1c•** based on the optimized geometry of the ground state.

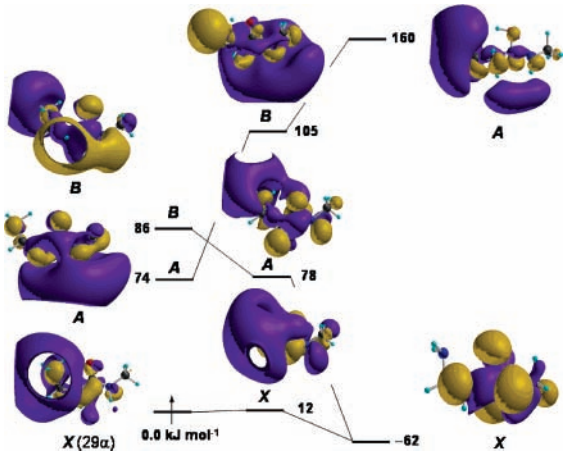

Figure 12. Correlation diagram for the H-atom migration in **1c•** → TS2 → **1f•**.

electronic states of the incipient radical **1c•**, and thus, the excited states may play a role in the radical dissociations. We studied by time-dependent DFT calculations the excitation energies and molecular orbitals pertinent to excited electronic states in **1c•** produced by vertical electron capture in $\mathbf{1c}^+$ and also for excitation from the relaxed **1c•** geometry. The excited-state energies for the *A*−*F* doublet states and molecular orbitals for *X*−*C* states in relaxed **1c•** are shown in Figure 11. The highest singly occupied molecular orbital (29α, SOMO) in the *X* state is a combination of an ammonium 3s Rydberg-like orbital (the main component) and an amide π-orbital. It should be noted that the energy gap between the SOMO and the underlying occupied 28α and 28β amide π-orbitals, $\Delta E = 5.80$ and 5.77 eV, respectively, is substantially greater than the 29α electron binding energy (3.4 eV). This implies that all one-electron excitations in **1c•** involve promotion of the 29α electron to the virtual orbital space. Likewise, electron capture in $\mathbf{1c}^+$ can involve only the virtual orbital space because excitation of the 28α or 28β electrons would lead to autoionizing states.

The first excited doublet state (*A*) is a combination of a Rydberg-like orbital, which is delocalized over the methylene side-chain groups, and the amide π-orbital. The *X*−*A* energy gap increases from 0.49 eV in vertically formed **1c•** to 0.77 eV in a relaxed radical. The *B* and higher excited states in **1c•** can be likewise represented as combinations of ammonium or methylene *n*s and *n*p Rydberg-like orbitals and the σ^* and π^* molecular orbitals of the amide group. The *A* and *B* states in vertically formed **1c•** were calculated to have long radiative lifetimes (>0.3 μs), which should be sufficient to allow the radicals to vibrationally relax to the corresponding potential energy minima. The latter have radiative lifetimes of >0.3 μs, as estimated from the calculated lifetimes of the *A* and *B* states by vertical excitation from the potential energy minimum of ground state **1c•**. Hence, the *A* and *B* states are estimated to have sufficiently long radiative lifetimes to participate in kinetically relevant dissociations in **1c•**.

Figure 12 shows a correlation diagram for the three lowest electronic states in **1c•**, TS2, and **1f•**. The *X* state develops an increasing π-orbital component at the amide group along the reaction coordinate, as also indicated by the calculated spin densities (Scheme 6) that show 34% of unpaired electron density at amide C, N, and O atoms in TS2. The closely spaced *A* and *B* states in **1c•** correlate with the *B* and *A* states, respectively, in TS2, as judged from the corresponding orbital nodalities. The correlation indicates that the activation energy for an H-atom migration in the *A* state should increase relative to that in the *X* state, whereas the same reaction in the *B* state decreases to become barrierless. We note that an exact comparison of the activation energies in the excited states is not possible from the current data because the state energies in Figure 12 are from vertical electron excitation and do not represent true stationary states. Nevertheless, the excited-state energies seem to indicate a facile, perhaps barrierless, H-atom migration in the *B* state of **1c•**.

The close spacing of the ground and excited electronic states in TS2 probably accounts for the failure of perturbation-based single-point energy calculations (vide supra). The 6-311+G(d,p) and 6-311++G(3df,2p) wave functions were tested and found stable with respect to perturbations described by the excitation eigenvector (see Tables S3−S6 in the Supporting Information). Thus, the problem may be in the accuracy of virtual orbital eigenvalues that affect the second-order energy corrections.[41]

In summarizing the results of RRKM calculations and excited-state analysis, one can conclude that ammonium H-atom loss most likely dominates dissociations occurring on the *X* state potential energy surface of **1c•**. However, isomerization to **1f•** is facile in the *B* state and may trigger other dissociations. According to Figure 12, an aminoketyl radical **1f•** produced from the *B* state of **1c•** is expected to have sufficient internal energy, >150 kJ mol^{-1}, to undergo isomerization to **2f•** followed by N−C_α dissociation by loss of the methyl group. The crossing point for it (k_9) and reverse H atom migration in **1f•** (k_5) is at $E_{int} = 115 + 71 = 186$ kJ mol^{-1} (Figure 10), and $k_9/k_5 = 0.4$ at $E_{int} = 150$ kJ mol^{-1}. This indicates that a fraction of **1c•** that was produced by electron capture in the *B* state can undergo N−C_a bond cleavage resulting in the loss of the methyl group (products **5** and **6**). Hence, the actual branching ratio for loss of H and CH_3 may depend on the population of the *X* and *B* electronic states upon electron capture.

Note that the $^+NR^+$ mass spectra of **1c•** (Figure 3a and Figures S1 and S2 in the Supporting Information) do not show a peak at *m*/*z* 88 that would indicate a loss of methyl and a presence of **5** or **6**. However, an enolimine analogous to **5** and **6** was reported to undergo extensive dissociation upon $^+NR^+$,[9] and so, the putative *m*/*z* 88 peak may be too small to be detected at the current signal-to-noise level.

Relevance to Dissociations of Peptide Radicals. The above-described detailed analysis of the energetics and kinetics of dissociations of β-alanine amide-derived radicals points to a competition between ammonium H-atom loss and transfer. H-atom loss is commonly observed upon ECD of peptide

cations,[42] and the present work indicates that it can readily occur from side-chain ammonium groups of lysine residues in spite of hydrogen bonding to the peptide backbone. In contrast, the present data indicate that the loss of ammonia is not competitive when occurring from the side-chain ammonium group. As reported previously, N-terminal ammonium groups in peptide radicals are extremely susceptible to highly exothermic elimination as ammonia that requires a very small activation energy and proceeds rapidly and spontaneously by out-of-plane rotation about the N-terminal $C_\alpha-C{=}O$ bond.[4,10] Hence, loss of ammonia from peptide ions upon ECD is likely to involve N-terminal amine groups.

The transition state energy for an ammonium H-atom transfer to an amide carbonyl shows dependence on the transition state geometry. From the hitherto studied models, it appears that the TS energies decrease as the size of the ring involving the migrating H atom increases, for example, from a five-membered transition state in an N-terminal ammonium,[4] through a six-membered ring in TS2, to a nine-membered transition state for an H-atom transfer from a lysine ϵ-ammonium group.[4,7] This finding is in line with the electron distribution in such transition states that can be described by the proton-coupled electron-transfer model, which favors a near collinear arrangement of the three atoms involved ($X\cdots H\cdots Y$).[43] The finding that H-atom transfer to the amide carbonyl can occur from a low-lying excited electronic state of an ammonium radical is significant because it can provide yet another pathway for the formation of aminoketyl radical intermediates that can trigger $N-C_\alpha$ bond dissociations.

Conclusions

Ammonium radicals **1c•** produced by femtosecond collisional electron transfer to protonated β-alanine N-methyl amide dissociate completely on the microsecond time scale. The competitive dissociation channels are difficult to discern in the neutralization−reionization mass spectra because of overlapping and convergent pathways. Ab initio calculations combined with RRKM kinetic analysis indicate that **1c•** should preferentially lose an ammonium hydrogen atom in dissociations proceeding on the ground electronic state. In contrast, the *B* excited electronic state of **1c•** is predicted to undergo a facile isomerization to an aminoketyl intermediate whose further dissociations by $N-C_\alpha$ bond cleavage would result in the loss of the amide methyl group.

Acknowledgment. Support of this work by the National Science Foundation (Grants CHE-0349595 for experiments and CHE-0342956 for computations) is gratefully acknowledged. The Computational Chemistry Center at the UW Department of Chemistry receives joint support by the NSF and University of Washington. Thanks are due to Dr. Martin Sadilek for technical assistance with mass spectra measurements. The Jeol HX-110 mass spectrometer was a generous donation from the former Seattle Biomembrane Institute courtesy of Professor S. Hakomori.

Supporting Information Available: Tables S1−S6 with calculated proton affinities, transition state energies, and stability calculations; Figures S1−S4 with neutralization−reionization mass spectra; and Schemes S1 and S2. This material is available free of charge via the Internet at http://pubs.acs.org.

References and Notes

(1) Zubarev, R. A.; Kelleher, N. L.; McLafferty, F. W. *J. Am. Chem. Soc.* **1998**, *120*, 3265−3266.

(2) Coon, J. J.; Ueberheide, B.; Syka, J. E. P.; Dryhurst, D. D.; Ausio, J.; Shabanowitz, J.; Hunt, D. F. *Proc. Natl. Acad. Sci. U.S.A.* **2005**, *102*, 9463−9468.

(3) Zubarev, R. A.; Horn, D. M.; Fridriksson, E. K.; Kelleher, N. L.; Kruger, N. A.; Lewis, M. A.; Carpenter, B. K.; McLafferty, F. W. *Anal. Chem.* **2000**, *72*, 563−573.

(4) Tureček, F.; Syrstad, E. A. *J. Am. Chem. Soc.* **2003**, *125*, 3353−3369.

(5) Syrstad, E. A.; Tureček, F. *J. Am. Soc. Mass Spectrom.* **2005**, *16*, 208−224.

(6) Sobczyk, M.; Simons, J. *J. Phys. Chem. B* **2006**, *110*, 7519−7527.

(7) Tureček, F. *J. Am. Chem. Soc.* **2003**, *125*, 5954−5963.

(8) Bakken, V.; Helgaker, T.; Uggerud, E. *Eur. J. Mass Spectrom.* **2004**, *10*, 625−638.

(9) Syrstad, E. A.; Stephens, D. D.; Tureček, F. *J. Phys. Chem. A* **2003**, *107*, 115−126.

(10) Tureček, F.; Syrstad, E. A.; Seymour, J. L.; Chen, X.; Yao, C. *J. Mass Spectrom.* **2003**, *38*, 1093−1104.

(11) Chen, X.; Tureček, F. *J. Am. Chem. Soc.* **2006**, *128*, 12520−12530.

(12) Yao, C.; Fung, Y. M. E.; Tureček, F. Presented at the UPPCON IV Conference, Hong Kong, December 2006.

(13) (a) Curtis, P. M.; Williams, B. W.; Porter, R. F. *Chem. Phys. Lett.* **1979**, *65*, 296−299. (b) Burgers, P. C.; Holmes, J. L.; Mommers, A. A.; Terlouw, J. K. *Chem. Phys. Lett.* **1983**, *102*, 1−3. (c) Danis, P. O.; Wesdemiotis, C.; McLafferty, F. W. *J. Am. Chem. Soc.* **1983**, *105*, 7454−7456. For recent reviews, see (d) Zagorevskii, D. V. In *Comprehensive Coordination Chemistry II*; McCleverty, J. A., Meyer, T. J., Eds.; Elsevier: Oxford, 2004; pp. 381−386. (e) Tureček, F. In *Encyclopedia of Mass Spectrometry*; Armentrout, P. B., Ed.; Elsevier: Amsterdam, 2003; Vol. 1, Chapter 7, pp 528−541. (f) Tureček, F.; *Top. Curr. Chem.* **2003**, *225*, 77−129. (g) Zagorevskii, D. V. *Coord. Chem. Rev.* **2002**, *225*, 5−34. (h) Gerbaux, P.; Wentrup, C.; Flammang, R. *Mass Spectrom. Rev.* **2000**, *19*, 367−389. (i) Zagorevskii, D. V.; Holmes, J. L. *Mass Spectrom. Rev.* **1999**, *18*, 87−118. (j) Schalley, C.; Hornung, G.; Schröder, D.; Schwarz, H. *Chem. Soc. Rev.* **1998**, *27*, 91−104.

(14) Robinson, A. B.; Robinson N. E. *Molecular Clocks: Deamidation of Asparaginyl and Glutaminyl Residues in Peptides and Proteins*; Althouse Press: Cave Junction, OR, 2004.

(15) (a) Uhlmann, E.; Peyman, A.; Breipohl, G.; Will, D. W. *Angew. Chem., Int. Ed. Engl.* **1998**, *37*, 2796−2823. (b) Decker, E. A.; Chan, W. K. M.; Mei, L.; Mcneill-Tompkins, G. L.; Livisay, S. A. In *Natural Antioxidants*; Shahidi, F., Ed.; AOCS Press: Champaign, IL, 1997; pp 271−282. (c) Lane, M. D. In *Encyclopedia of Biological Chemistry*; Elsevier: Oxford, 2004; Vol. 1, pp 475−477.

(16) Chow, H.-F.; Mong, T. K. K.; Chan, Y.-H.; Cheng, C. H. K. *Tetrahedron* **2003**, *59*, 3815−3820.

(17) Smith, E. L.; Slonim, N. B. *J. Biol. Chem.* **1948**, *176*, 835−841.

(18) Harrison, A. G. *Chemical Ionization Mass Spectrometry*, 2nd ed.; CRC Press: Boca Raton, FL, 1992.

(19) Wolken, J. K.; Tureček, F. *J. Phys. Chem. A* **1999**, *103*, 6268−6281.

(20) (a) Tureček, F.; Gu, M.; Shaffer, S. A. *J. Am. Soc. Mass Spectrom.* **1992**, *3*, 493−501. (b) Tureček, F. *Org. Mass Spectrom.* **1992**, *27*, 1087−1097.

(21) Seymour, J. L.; Syrstad, E. A.; Langley, C. C.; Tureček, F. *Int. J. Mass Spectrom.* **2003**, *228*, 687−702.

(22) Chen, X.; Syrstad, E. A.; Nguyen, M. T.; Gerbaux, P.; Tureček, F. *J. Phys. Chem A* **2005**, *109*, 8121−8132.

(23) Frisch, M. J.; Trucks, G. W.; Schlegel, H. B.; Scuseria, G. E.; Robb, M. A.; Cheeseman, J. R.; Montgomery, J. A., Jr.; Vreven, T.; Kudin, K. N.; Burant, J. C.; Millam, J. M.; Iyengar, S. S.; Tomasi, J.; Barone, V.; Mennucci, B.; Cossi, M.; Scalmani, G.; Rega, N.; Petersson, G. A.; Nakatsuji, H.; Hada, M.; Ehara, M.; Toyota, K.; Fukuda, R.; Hasegawa, J.; Ishida, M.; Nakajima, T.; Honda, Y.; Kitao, O.; Nakai, H.; Klene, M.; Li, X.; Knox, J. E.; Hratchian, H. P.; Cross, J. B.; Adamo, C.; Jaramillo, J.; Gomperts, R.; Stratmann, R. E.; Yazyev, O.; Austn, A. J.; Cammi, R.; Pomelli, C.; Ochterski, J. W.; Ayala, P. Y.; Morokuma, K.; Voth, G. A.; Salvador, P.; Dannenberg, J. J.; Zakrzewski, V. G.; Dapprich, S.; Daniels, A. D.; Strain, M. C.; Farkas, O.; Malick, D. K.; Rabuck, A. D.; Raghavachari, K.; Foresman, J. B.; Ortiz, J. V.; Cui, Q.; Baboul, A. G.; Clifford, S.; Cioslowski, J.; Stefanov, B. B.; Liu, G.; Liashenko, A.; Piskorz, P.; Komaromi, I.; Martin, R. L.; Fox, D. J.; Keith, T.; Al-Laham, M. A.; Peng, C. Y.; Nanayakkara, A.; Challacombe, M.; Gill, P. M. W.; Johnson, B.; Chen, W.; Wong, M. W.; Gonzalez, C.; Pople, J. A. *Gaussian 03*, Revision B.05; Gaussian, Inc.; Pittsburgh, PA, 2003.

(24) (a) Becke, A. D. *J. Chem. Phys.* **1993**, *98*, 1372−1377. (b) Becke, A. D. *J. Chem. Phys.* **1993**, *98*, 5648−5652. (c) Stephens, P. J.; Devlin, F. J.; Chabalowski, C. F.; Frisch, M. J. *J. Phys. Chem.* **1994**, *98*, 11623−11627.

(25) Tureček, F.; Cramer, C. J. *J. Am. Chem. Soc.* **1995**, *117*, 12243−12253.

(26) (a) Schlegel, H. B. *J. Chem. Phys.* **1986**, *84*, 4530−4534. (b) Mayer, I. *Adv. Quantum Chem.* **1980**, *12*, 189−262.

(27) (a) Tureček, F. *J. Phys. Chem. A* **1998**, *102*, 4703−4713. (b) Tureček, F.; Polášek, M.; Frank, A. J.; Sadílek. M. *J. Am. Chem. Soc.* **2000**, *122*, 2361−2370. (c) Polášek, M.; Tureček, F. *J. Am. Chem. Soc.* **2000**, *122*, 9511−9524. (d) Tureček, F.; Yao, C. *J. Phys. Chem. A* **2003**, *107*, 9221−9231. (e) Rablen, P. R. *J. Am. Chem. Soc.* **2000**, *122*, 357−368. (f) Rablen, P. R. *J. Org. Chem.* **2000**, *65*, 7930−7937. (g) Rablen, P. R.; Bentrup, K. H. *J. Am. Chem. Soc.* **2003**, *125*, 2142−2147. (h) Hirama, M.; Tokosumi, T.; Ishida, T.; Aihara, J. *Chem. Phys.* **2004**, *305*, 307−316.

(28) Čížek, J.; Paldus, J.; Šroubková, L. *Int. J. Quantum Chem.* **1969**, *3*, 149−167.

(29) Purvis, G. D.; Bartlett, R. J. *J. Chem. Phys.* **1982**, *76*, 1910−1918.

(30) Curtiss, L. A.; Raghavachari, K.; Pople, J. A. *J. Chem. Phys.* **1993**, *98*, 1293−1298.

(31) Pople, J. A.; Head-Gordon, M.; Raghavachari, K. *J. Chem. Phys.* **1987**, *87*, 5968−5975.

(32) (a) Boldyrev, A. I.; Simons, J. *J. Chem. Phys.* **1992**, *97*, 6621−6627. (b) Shaffer, S. A.; Tureček, F. *J. Am. Chem. Soc.* **1994**, *116*, 8647−8653. (c) Nguyen, V. Q.; Sadílek, M.; Frank, A. J.; Ferrier, J. G.; Tureček, F. *J. Phys. Chem. A* **1997**, *101*, 3789−3799. (d) Yao, C.; Tureček, F. *Phys. Chem. Chem. Phys.* **2005**, *7*, 912−920.

(33) Stratmann, R. E.; Scuseria, G. E.; Frisch, M. J. *J. Chem. Phys.* **1998**, *109*, 8218−8224.

(34) Reed, A. E.; Weinstock, R. B.; Weinhold, F. *J. Chem. Phys.* **1985**, *83*, 735−746.

(35) Gilbert, R. G.; Smith, S. C. *Theory of Unimolecular and Recombination Reactions*; Blackwell Scientific Publications: Oxford, 1990; pp 52−132.

(36) Zhu, L.; Hase, W. L. *Quantum Chemistry Program Exchange*; Indiana University: Bloomington, 1994; Program No. QCPE 644.

(37) Frank, A. J.; Sadílek, M.; Ferrier, J. G.; Tureček, F. *J. Am. Chem. Soc.* **1997**, *119*, 12343−12353.

(38) Standard Reference Database Number 69, March, 2003, Release; http://webbook.nist.gov/chemistry.

(39) Wu, J.; Gard, E.; Bregar, J.; Green, M. K.; Lebrilla, C. B. *J. Am. Chem. Soc.* **1995**, *117*, 9900−9905.

(40) (a) Wolken, J. K.; Tureček, F. *J. Am. Chem. Soc.* **1999**, *121*, 6010−6018. (b) Tureček, F. *Int. J. Mass Spectrom.* **2003**, *227*, 327−338.

(41) Møller, C.; Plesset, M. C. *Phys. Rev.* **1934**, *46*, 618−622.

(42) Cooper, H. J.; Hudgins, R. R.; Håkansson, K.; Marshall, A. G. *J. Am. Soc. Mass Spectrom.* **2002**, *13*, 241−249.

(43) Siegbahn, P. E. M.; Eriksson, L.; Himo, F.; Pavlov, M. *J. Phys. Chem. B* **1998**, *102*, 10622−10629.